J Biomol NMR (2011) 51:283–292
DOI 10.1007/s10858-011-9535-z

ARTICLE

Cryogenic temperature effects and resolution upon slow cooling of protein preparations in solid state NMR

Arne H. Linden · W. Trent Franks · Ümit Akbey · Sascha Lange · Barth-Jan van Rossum · Hartmut Oschkinat

Received: 7 December 2010 / Accepted: 18 July 2011 / Published online: 9 August 2011

Abstract X-ray crystallography using synchrotron radiation and the technique of dynamic nuclear polarization (DNP) in nuclear magnetic resonance (NMR) require samples to be kept at temperatures below 100 K. Protein dynamics are poorly understood below the freezing point of water and down to liquid nitrogen temperatures. Therefore, we investigate the α-spectrin SH3 domain by magic angle spinning (MAS) solid state NMR (ssNMR) at various temperatures while cooling slowly. Cooling down to 95 K, the NMR-signals of SH3 first broaden and at lower temperatures they separate into several peaks. The coalescence temperature differs depending on the individual residue. The broadening is shown to be inhomogeneous by hole-burning experiments. The coalescence behavior of 26 resolved signals (of 62) was compared to water proximity and crystal structure Debye–Waller factors (B-factors). Close proximity to the solvent and large B-factors (i.e. mobility) lead, generally, to a higher coalescence temperature. We interpret a high coalescence temperature as indicative of a large number of magnetically inequivalent populations at cryogenic temperature.

Keywords Cryogenic NMR spectroscopy · Low-temperature dynamics · Solvent effects · Protein glass transition · Coalescence

Electronic supplementary material The online version of this article (doi:10.1007/s10858-011-9535-z) contains supplementary material, which is available to authorized users.

A. H. Linden · W. T. Franks · Ü. Akbey · S. Lange · B.-J. van Rossum · H. Oschkinat (✉)
Forschungsinstitut für Molekulare Pharmakologie (FMP), Robert-Rössle-Straße 10, 13125 Berlin, Germany
e-mail: oschkinat@fmp-berlin.de

Introduction

Solid state nuclear magnetic resonance (ssNMR) has been utilized to determine structures of a number of proteins (SH3 (Castellani et al. 2002, 2003), Kaliotoxin (Lange et al. 2005), Ubiquitin (Zech et al. 2005), GB1 (Franks et al. 2008; Zhou et al. 2007)) including fibrillar (Amyloid Beta (Petkova et al. 2002), Het-S (Wasmer et al. 2008), Alpha-Synuclein (Heise et al. 2005)) and oligomeric (Crh (Loquet et al. 2008), α-B Crystallin (Jehle et al. 2010, 2009)) systems. Cryogenic ssNMR has been used for trapping intermediate states of for example protein metal centers (Lipton et al. 2009) or functional states of membrane-proteins (Gansmüller et al. 2009). However, in many cases the low sensitivity of ssNMR limits biological investigations. Dynamic nuclear polarization (DNP) enhances the signal to noise ratio with the condition that the spin relaxation times are long enough for efficient transfer of electron polarization to the nuclei of interest, requiring cryogenic temperatures around 100 K (Akbey et al. 2010a,b; Barnes et al. 2009; Lesage et al. 2010). Cryogenic temperatures are also required for X-ray crystallography using synchrotron radiation to protect against radiation-damage. Nevertheless, dynamic processes in hydrated proteins at low temperatures are not fully understood, and therefore it is desirable to investigate effects of slow cooling at atomic resolution within the temperature range from 95 to 295 K.

Protein structures determined at ambient (NMR) or cryogenic temperatures (crystallography) are remarkably similar (Franks et al. 2008). Small structural differences can often be attributed to the different kinds of distance averaging inherent in each method. The techniques also have different timescales of measured dynamics. NMR-spectroscopists normally categorize slow (seconds to

milliseconds), intermediate (microseconds) and fast (nanoseconds and below) dynamics regimes (Spiess 1985).

Dynamics of hydrated proteins upon cooling are influenced by effects such as: I) the bulk solvent forming an ice or glass matrix, II) the solvent-accessible side chains interacting with hydration shell solvent molecules and III) the solvent independent thermal motions of the protein itself (i.e. side chain rotations, librations, and low-frequency breathing modes) (Siemer et al. 2010). These processes affect the observed NMR protein signals and may interfere with the experimental design, one example is the performance of hetero-nuclear decoupling (Bajaj et al. 2009). Additionally, the rate of freezing may determine the resulting states. The submersion of 3.2 mm ssNMR rotors in liquid nitrogen results in cooling rates of ca. 10°C per second (Hu et al. 2009). Specialized techniques have arisen to improve the freezing rate, which were not investigated in this study (see Kriminski et al. 2003). The literature discusses a "caging" of proteins at low temperatures by immobilized solvent (water) molecules as well as an occurrence of a "protein glass transition temperature" (T_g) around −73°C (200 K) in water (Ngai et al. 2008). Below T_g the influence of the solvent is reduced while the intrinsic dynamics of the protein become more important. Primarily dynamics of methyl groups are observed between T_g and 100 K (Bajaj et al. 2009; Vugmeyster et al. 2010) in both hydrated and water-free proteins by neutron scattering (Roh et al. 2005). Samples without methyl groups do not show such dynamics below T_g (Caliskan et al. 2006; Ngai et al. 2008). Aromatic side chain ring-flips enter slow dynamics at low temperatures, which improves the sensitivity of the ring-atoms, probably due to improved cross polarization (CP) (Bajaj et al. 2009). All these issues aside, room temperature quality spectra have been obtained at 90 K for the water-free tri-peptide MLF (Bajaj et al. 2009) and at 180 K for the protein GB1 (Franks et al. 2005). However, recent work has shown that individual NMR signals of hydrated proteins broaden to 2–3 ppm linewidth at liquid helium temperatures (Hu et al. 2009; Thurber and Tycko 2008).

Generally, there are two types of spectral broadening (Maricq and Waugh 1979): Inhomogeneous broadening in protein NMR arises from the presence of multiple static conformers on the timescale of the measurement and is identified by a narrow diagonal, a longer T_2 than indicated by the linewidth and the possibility to burn a hole in the spectrum. In contrast, homogeneous broadening arises from an increase in the natural linewidth and is indicated by a broad diagonal, a T_2 consistent with the observed linewidth and the inability to burn a hole in the spectrum. Inhomogeneous broadening is generally addressed by improved sample preparation, while the presence of homogeneous broadening is a fundamental limitation.

In this work, we study the changes in NMR spectra of microcrystalline samples of the α-spectrin SH3 domain upon cooling to 95 K. We investigate the type of broadening and the dynamics underlying this process. In fact, inhomogeneous broadening dominates and it is likely that multiple sidechain conformations are frozen out. We investigate further the influence of the surrounding solvent on the broadening. In principle, we demonstrate the possibility to record resolved solid-state NMR-data at cryogenic temperatures. All this information is valuable for future NMR experiments of hydrated protein samples at cryogenic temperatures, for example the growing number of cryogenic DNP-investigations.

Experimental section

Protonated SH3 was grown in *E. coli* in minimal media with $^{1}H_2O$, $^{15}NH_4Cl$, and ^{13}C glucose, purified, precipitated, and transferred into the NMR rotor as described elsewhere (Pauli et al. 2001). Deuterated SH3 was grown in a similar manner, except for use of a $^{2}H_2O$ buffer and an extended growth and induction time due to the $^{2}H_2O$ media. The deuterated sample was then placed in a $^{1}H_2O$ solution or $^{1}H_2O/^{2}H_2O$ mixture to replace exchangeable ^{2}H with ^{1}H (Akbey et al. 2010a, b, 2009).

All spectra were obtained on a Bruker AVANCE III 400 MHz spectrometer with Topspin version 2.1. A Bruker DNP-cryo-probe for 3.2 mm rotors tuned to HCN was used. The samples were all held in standard Bruker 3.2 mm diameter Zirconium rotor with vespel spinning cap and a silicon rubber seal immediately below the cap. All spectra are referenced to the adamantane downfield peak (40.48 ppm) at room temperature (Morcombe and Zilm 2003). A Bruker Cryo-NMR cooling cabinet was used to independently control the bearing, variable temperature (VT) and drive nitrogen gas streams to the indicated temperatures. At the lowest temperature (96 K) the gas streams were controlled at 96 K (VT), 100 K (bearing) and 105 K (drive). The sample temperatures were verified following the method of Thurber and Tycko (2009). At the lowest reported temperature, 96 K, the sample temperature was determined to be 103.5 K; with gas streams of 295 K the sample temperature was 299 K. The frictional heating due to magic angle spinning (MAS) is below 5 K except at the lowest temperature, where it was slightly larger since not all gas streams could be controlled sufficiently. The measured sample temperatures were, in all cases, close to the temperature of the exhausting gas. A Bruker MAS-unit controlled the spinning frequency at 8,889 ± 2 Hz. The instrument was allowed to equilibrate at least 20 min at each temperature before the tuning, decoupling, CP match conditions and pulse widths were optimized. Optimization

of the shims on liquid n-pentane at 145 K did not improve the spectral quality of the protein sample compared to shims optimized at 273 K, which removes shimming as a significant source of line-broadening at low temperatures.

The parameters of the measurements are as follows: For the 1D spectra: 295–270 K each 32 scans, 4 s delay, CP contact time 1.5 ms; 253–133 and 293 K after cooling each 64 scans and 95 K 128 scans, 3 s delay, CP contact time 2 ms. No line broadening was used in processing.

The 2D proton-driven spin diffusion (PDSD) spectra (Bloembergen 1949; Szeverenyi et al. 1982) were recorded with 4 scans (173 K 8 scans), 1,186/512 points in the direct/indirect dimension. The CP contact time was 2 ms and the relaxation delay was set to 3 s or 1.3 times the measured T_1 time when T_1 is longer than 2.3 s. Spectra were recorded with 11.25 ms PDSD mixing, except on the deuterated sample where 50 ms of PDSD mixing were used.

Spectra were zero filled to 8 k points in the direct dimension and 4 k points in the indirect dimension and then line broadened with a Gaussian window (GM; 30 Hz, 0.1 top position) in the direct dimension and a sine squared function (qsine = 3) in the indirect dimension. In the detailed view of SH3 single resonances, the processing in both dimensions was changed to GM (8 Hz, 0.08 top position). For the observations of aromatic signals (SI Fig. 1) the processing was broadened to 40 Hz (0.05 top position) and 60 Hz (0.04 top position) in the direct and indirect dimension. Sparky was used to plot spectra and to calculate the noise (Goddard and Kneller). The base level of the spectra was set to 6 times the calculated noise (6σ) with contours drawn incremented by a factor 1.1.

Two crystal structures were used for the calculation of the B-value: at 100 K with a resolution of 1.49 Å (RCSB PDB: 1U06; Chevelkov et al. 2005) and at 293 K with 1.85 Å resolution (RCSB PDB: 2NUZ; Agarwal et al. 2007). The H-bonds between neighboring molecules were calculated with a flexibility of ±0.4 Å and ±20° (Mills and Dean 1996). Calculations and images were made using the UCSF Chimera package from the Resource for Biocomputing, Visualization, and Informatics at the University of California, San Francisco (supported by NIH P41 RR-01081; Pettersen et al. 2004) Assignments were taken from Pauli and Castellani (Castellani et al. 2003; Pauli et al. 2001). For the calculation of water-accessibility (WA) see Linser et al. 2009. The size of the globe for the calculations was changed from 4 to 1.4 Å to simulate a water molecule.

Results and discussion

The response to slow cooling is first demonstrated with 1D ^{13}C spectroscopy (Fig. 1). The spectrum at 295 K is representative of nano-crystalline SH3, where one-bond scalar

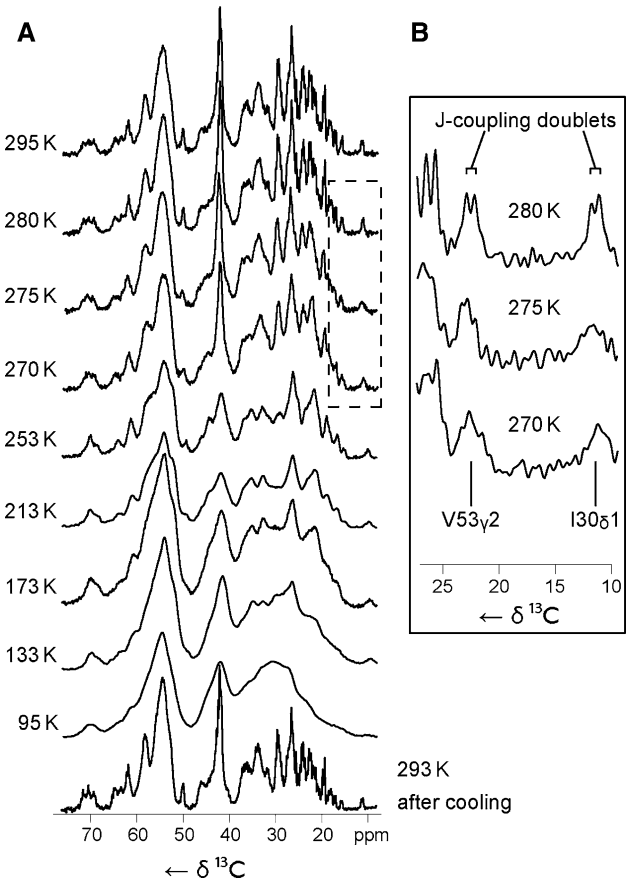

Fig. 1 **a** 1D ^{13}C CP spectra of the aliphatic region of SH3 at different temperatures. **b** Magnification of the isoleucine 30 Cδ1 and valine 53 Cγ2 resonances. The spectra are scaled according to the number of scans

couplings are identifiable on resolved resonances. At ~275 K the scalar coupling doublets are no longer resolved (Fig. 1b). As the temperature is further reduced, the 1D spectrum shows apparent broadening with a maximum of linewidth at 95 K. No step-like changes are observed in the 1D SH3 spectra at T_g (~200 K) upon slow cooling. After re-warming the sample to 293 K (Fig. 1, bottom), the spectrum regains its previous quality, with the same resolution and identical chemical shifts as the initial spectrum. The sample was temperature cycled at least five times, and the room temperature spectrum returned after each cycle. Therefore, the tertiary structure and nano-crystalline state of SH3 must be preserved through these freeze–thaw cycles. The global proton spin–lattice relaxation time (T_1) ranges from 0.50 s (293 K) to 13 s (98 K) as measured by proton inversion-recovery and subsequent proton-carbon CP.

2D spectroscopy

2D ^{13}C–^{13}C PDSD (Bloembergen 1949; Szeverenyi et al. 1982) spectra (Fig. 2) were collected to investigate the

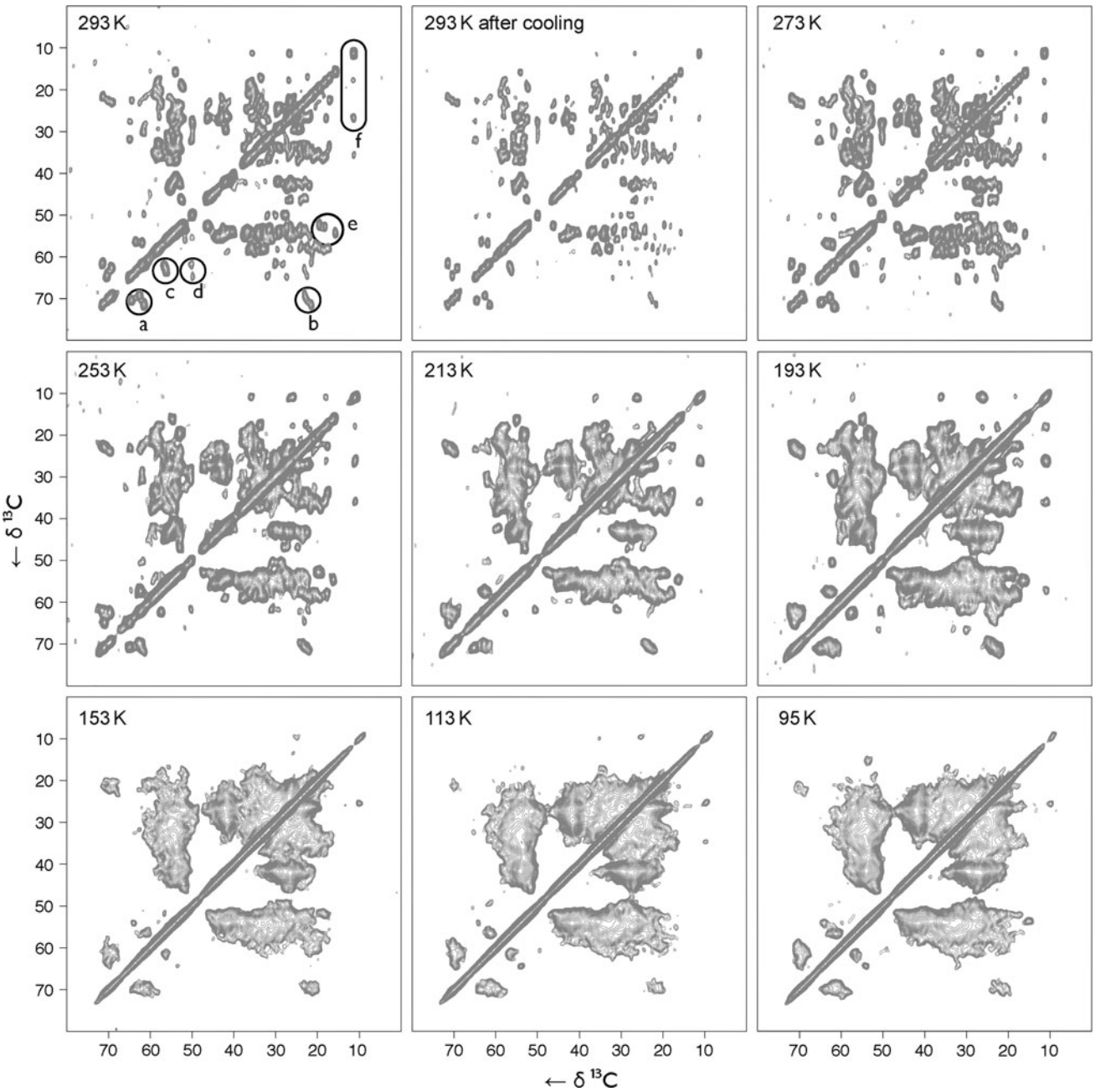

Fig. 2 2D ^{13}C–^{13}C PDSD spectra of SH3 recorded at indicated temperatures. All spectra were recorded with 2 ms CP and 11.25 ms PDSD mixing (50 ms for the deuterated sample). Marked regions are discussed in the text or shown in Fig. 3 (**a** Thr Cβ–Cα; **b**: Thr Cβ–Cγ; **c**: Ser Cβ–Cα; **d**: Pro Cα–Cδ; **e**: Ala Cα–Cβ; **f**: Ile Cδ1, Cδ1–Cγ2, Cδ1–Cγ2). The base level of all spectra is set to 6σ of the noise

behavior of individual resonances. Generally, the spectra broaden until each resonance reaches its individual coalescence temperature, and then it splits into multiple signals. At low temperatures (153–96 K, depending on the individual residue) the single peaks have a similar linewidth as the motionally averaged peaks at 293 K. The autocorrelation signals are not greatly broadened at low temperatures as measured perpendicular to the diagonal. This in an additional indicator for inhomogeneous broadening. Furthermore, cooling the sample faster by immersion in liquid nitrogen did not change the 1D and 2D spectra recorded at 95 K substantially.

Signal multiplication leads to poor apparent resolution in much of the spectrum. To avoid interferences due to signal overlap, we analyzed the spectral regions with well resolved peaks at room temperature such as: threonine

Cβ–Cα and Cβ–Cγ (T24, T32, T37), serine Cβ–Cα cross peaks (S19, S36), proline Cα–Cδ (P20, P54), alanine Cα–Cβ (A11, A55, A56), and cross peaks involving isoleucine Cδ1 (I30) (Fig. 2 top left, a–f; Fig. 3). Three of four threonines are typically visible at room temperature in CP based ^{13}C–^{13}C spectra of SH3; the fourth (T4) is visible in direct excitation experiments, and may contribute signal intensity at low temperatures. The Cβ–CO, Cβ–Cα and Cβ–Cγ cross peaks of the threonine residues are shown in the first three columns of Fig. 3. The signals broaden as the temperature is lowered, and then split into several distinct peaks. T37 is the last to broaden; it has a larger intensity at 193 K than the other resonances (2.5/3.8 times stronger than to T32/T24). The proline Cα–Cδ signals (fourth column) are single peaks at 293 K. At 253 K, P20 has broadened below detection, and does not return at lower temperatures. P54 on the other hand, is observed until 193 K, and then again at 113 K as a group of peaks. Alanine Cα–Cβ signals (fifth column) are observed to undergo coalescence as well. A55 is no longer observed at 153 K, but is observed again as at least three peaks at 95 K. A11 and A56 broaden and merge into one peak at 253 K, disappear around 113 K and reappear as multiple individual peaks at 95 K. In both cases of the reappearing proline and alanine peaks we made the assignment by analogy to room temperature data, as no other cross-peaks are detected at similar chemical shifts at room temperatures. The isoleucine (I30) cross peaks in SH3, involving Cδ (SI figure 2), remain homogeneous until 193 K. The cross peaks are observed throughout the full temperature range. Nevertheless they are affected by slight homogeneous broadening. The aromatic region (110–165 ppm) shows weak cross peaks at 293 K, but they appear more intensely at low temperatures (SI figure 1). For 3 tyrosine residues in SH3, we count at minimum 6 signal sets at 96 K. The aromatic spin systems are strongly coupled and are generally in a two site ring-flip dynamic state. The spectra suggest that the dynamics of the aromatic rings change from the intermediate regime at room temperature to slow at low temperatures and therefore more cross peaks are detectable.

The CO–Cα signals are mostly unresolved, even at room temperature. The only resolved CO–Cα cross peaks are those of P20, P54, and G51. The proline signals are broadened while cooling but still detectable at 95 K. We did not observe the bulk of CO–Cα signals to broaden in the same manner. The glycine 51 CO–Cα peak is detectable at all temperatures at mostly unchanged intensity, but it shows a weak splitting into multiple signals at low temperatures. This might be first evidence that the backbone is less inhomogeneously broadened than the sidechains. However, further investigations are needed to address this question.

Hole-burning spectroscopy

To further determine the nature of broadening observed in the SH3 spectra we applied hole-burning spectroscopy to the ^{13}C 1D spectra. For this purpose the carbon magnetization was stored along the longitudinal axis and within this time a 10 ms square pulse with low power was applied on the ^{13}C channel (see SI figure 3). We were able to burn a hole into the carbon spectrum at several temperatures for the Cα, carbonyl and methyl region (Fig. 4; 293 and 98 K shown). Each hole has comparable linewidth (half depth, carbonyl: 129 Hz at 293 K; 137 Hz at 98 K) and depth at both temperatures. This corroborates the notion that inhomogeneous broadening is the dominant type of broadening for the observable signals.

Deuteration

We used deuterated SH3 samples (Akbey et al. 2010a, b, 2009) to investigate the possibility that insufficient proton decoupling is the dominant contribution to linewidth at low temperatures. We recorded 2D spectra at low temperatures with fully deuterated samples where the exchangeable sites are protonated to allow proton-carbon CP (SI figure 4). We used a longer PDSD mixing time of 50 ms instead of 11.25 ms to compensate for the lower number of protons. Although fewer cross-peak signals are detectable compared to spectra of fully protonated samples it is evident that the inhomogeneous broadening is largely unchanged between deuterated and protonated samples. We conclude that insufficient decoupling is not a substantial part of the broadening observed with protonated samples.

Structural aspects

The behavior of individual resonances differs even amongst the same residue type. It is likely that the local environment mediates this temperature dependence; therefore we will discuss signal broadening and multiplication with regards to the local structure of the resonance in question. Well-resolved signals, such as T, A, and S, can be monitored throughout the entire temperature series. Other aliphatic carbon–carbon peaks, however, can only be monitored unambiguously to 213 K.

Of the four threonines in SH3, only three are observed in room temperature CP spectra. T4 is in a mobile loop region, and is not observed, although it may contribute to intensity at low temperatures. T24 (WA 0.3–0.8 Å; B-value 12.02) is in a loop without stabilizing factors. T32 (WA 0–0.3 Å; B-value 14.15, compare Fig. 5b) is located in a β-sheet with a hydrogen bond to N38 of an adjacent SH3-molecule. Thus T32 is part of a H-bond network and the degree of motion is hindered. The last threonine, T37 (WA

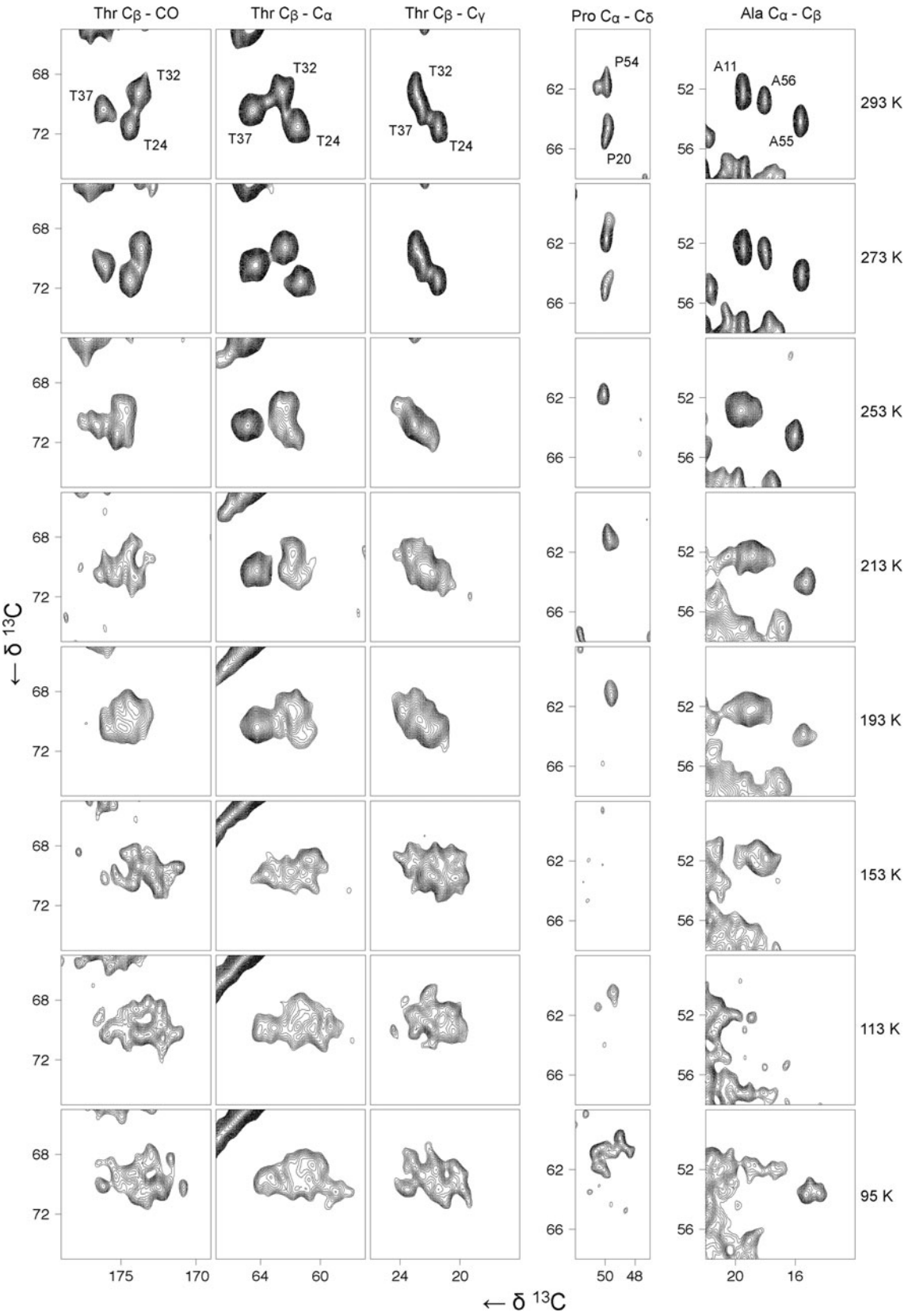

Fig. 3 2D ^{13}C–^{13}C PDSD spectra of the Thr, Pro, and Ala side chain regions at temperatures indicated

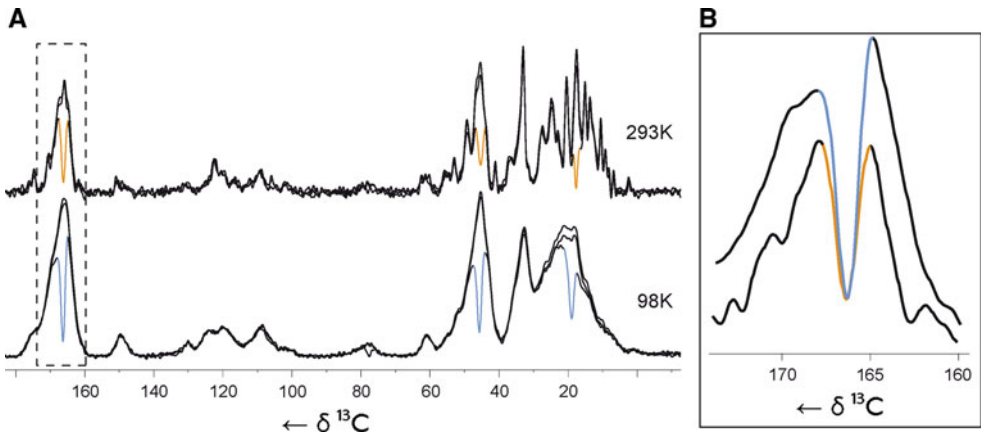

Fig. 4 **a** Three spectra of SH3 at 293 K (*top*) and three at 98 K (*bottom*). **a** long pulse of 10 ms at 42.25 dB power (471 Hz) was used to "burn holes" at three different carrier frequencies, colored with *orange* (293 K) or *blue* (98 K). **b** Detailed view of the carbonyl region

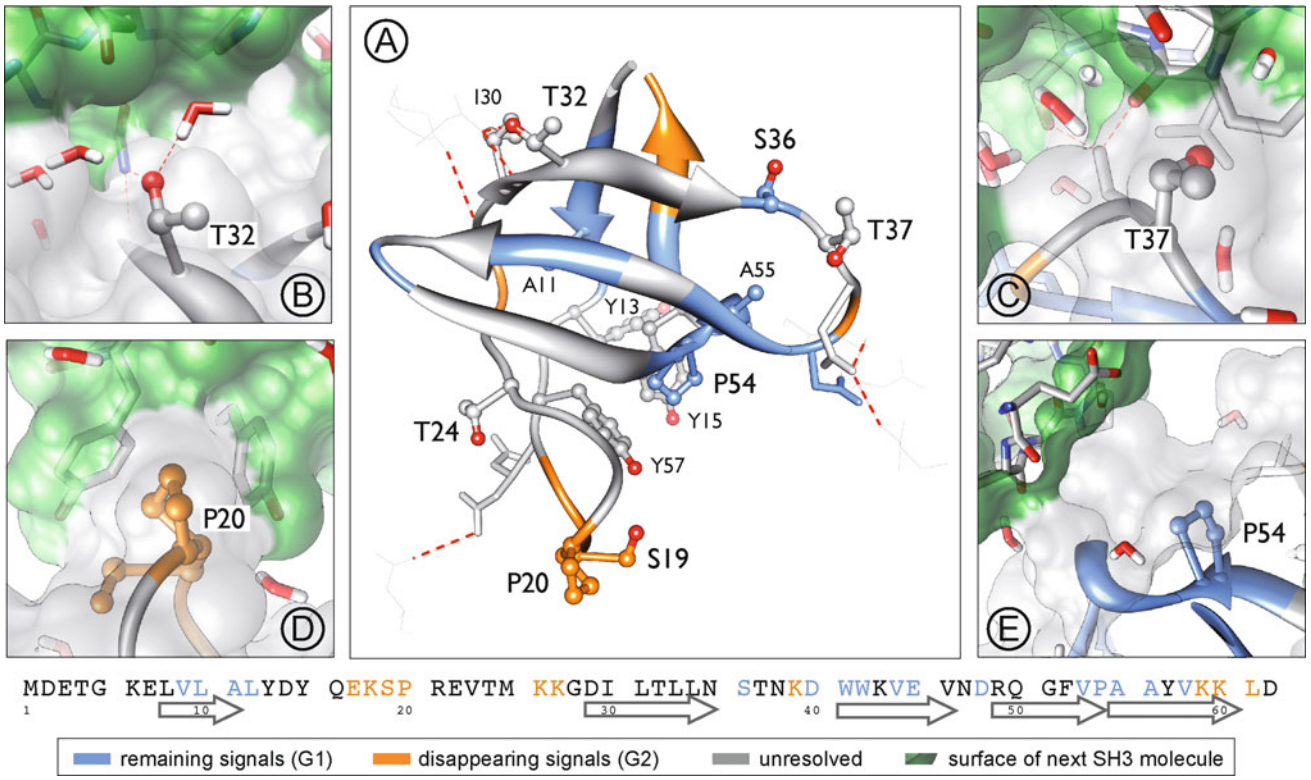

Fig. 5 **a** The crystal structure of SH3, surrounded by 14 molecules of a simulated crystal (rendered as surfaces; RCSB PDB: 1U06; Chevelkov et al. 2005). Residues are color-coded according to their NMR characteristics at different temperatures; residues for which the NMR signals remain between 293 and 213 K are colored *blue*; residues for which the cross peaks disappear in this range are colored *orange*; The four close-up views show T32 (**b**), T37 (**c**), P20 (**d**), and P54 (**e**) with their direct intermolecular environment (neighboring SH3 molecules: *green surfaces*), including crystal associated water molecules. The primary sequence of SH3 is plotted at the bottom. *Arrows* indicate β-strands; the *same color*-coding is used as in the structure

1–1.5 Å; B-value 9.81; compare Fig. 5c), is in a loop but also in a crystal contact. It is located in a cleft in the first hydration shell of an adjacent SH3 molecule. Another difference between T37 and the other two observed threonines in the χ_1 angle of +59° (T32: −5°; T24: −66°; out of the 1.49 Å crystal structure at 100 K; Chevelkov et al. 2005) Therefore, the methyl group of T37 is close to the backbone NH and not to the backbone CO. This might hinder the side chain motions and lead to a lower coalescence temperature. If multiple conformations are the source of the spectral broadening, it is reasonable to assume that the signals of T24 coalesce at a higher temperature than the signals of T32 and T37. Indeed the observed order of coalescence temperatures is: T37

(220 K) < T32 (246 K) < T24 (253 K), measured as the average coalescence temperature of the three cross peaks (Fig. 3).

Of the two prolines, P54 (B-value 12.18, compare Fig. 5e) is in a β-sheet and its side chain is oriented towards the core of the domain. Its signals remain until 193 K and then return at 113 K. In contrast, the resonances from the second proline, P20 (B-value 14.58, compare Fig. 5d), are not detected below 273 K. This proline is situated in a loop sandwiched by two tyrosines of an adjacent SH3-molecule. Due to the various conformers and ring-flip states of these two tyrosines, the flexibility of the loop region and the proline ring-pucker itself, many magnetically inequivalent environments are populated. Thus we attribute the higher coalescence temperature and the broader coalescence range to the greater number of populated states.

The three alanines show a temperature response similar to that of P54. A11 is in the middle of a β-sheet while the other two residues are situated in a turn between β-sheets. The A55 and A56 Cα–Cβ signals are already in coalescence at 153 K, while the A11 signal is still well above the noise threshold. At 113 K the resonances of all alanines show poor signal to noise. However, at 95 K, each alanine Cα–Cβ returns as a multitude of signals.

It is also possible to track several additional ^{13}C resonances from 293 to 213 K. However, due to the proximity of nearby peaks and the ambiguity of assigning multiple peaks, many resonances are excluded due to overlap, with only 26 of 62 residues unambiguously tracked to 213 K (which excludes the 3 threonines previously discussed, but includes the serines and prolines). The noise of each spectrum was calculated and the first contour level was drawn at 6 times the noise (6σ). If an individual peak appears above the 6σ threshold at every temperature between 293 and 213 K, it is assigned to group 1 (**G1**). Any resonance that falls below the threshold in this temperature range is placed into group 2 (**G2**). We interpret the vanishing signals as a measure for high temperature coalescence.

These results are mapped onto the crystal structure of SH3 (Fig. 5). 10 of 26 residues are classified into **G2**. These residues are found primarily in loop regions (Fig. 5, orange residues), e.g. between E17 to P20. However, K59 and K60 are found in a β-strand at the C-terminus. All 16 residues of **G1** are found in, or one residue away from, β-strands (Fig. 5, blue residues). Of the identifiable residues in the β-strands, 12 show remaining signals, whereas two at the C-terminus fall below the 6σ threshold.

We calculated the water-accessibility (WA) of single residues (Linser et al. 2009) and averaged the values for the two groups (Table 1). For the residues with disappearing signals (**G2**) we calculated an average distance of 0.88 Å to the solvent (with a maximum of 2.15 Å). **G1** residues show an averaged distance of 2.16 Å. The individual values are distributed over the full range of calculated values (0–5.3 Å). This suggests that the surrounding water plays an important role in the observed changes in linewidth. This hypothesis is supported by other studies with water-free samples that show less line broadening in 1D-spectra and less severe in 2D spectra (Bajaj et al. 2009).

Table 1 Average water accessibility [Å] calculated with the crystal structure at 293 K (Agarwal et al. 2007) and Debye–Waller-factors [Å^2] of side chain atoms of the crystal structure at 100 K (Chevelkov et al. 2005)

	Water accessibility [Å]	Debye–Waller-factor (B-values; [Å^2])
Extrema	0–5.3	9.81–28.93
Average of all side chains	1.38 ± 1.1	16.70 ± 5.2
Average of NMR signals detectable until 213 K; (**G1**)	2.16 ± 1.4	14.91 ± 3.7
Average of NMR signals not detectable until 213 K; (**G2**)	0.88 ± 0.7	19.81 ± 3.8

The error margins represent the standard deviation of the calculated accessibility and B-value averages

Small Debye–Waller-factors (B-values; Debye 1913; Waller 1923) of X-ray crystal structures are an index for rigidity. A comparison of the B-factors of the side chain atoms (excluding the N, CO, and Cα of the backbone; Agarwal et al. 2007; Chevelkov et al. 2005) for **G1** and **G2** is shown in Table 1. The values corresponding to **G1** signals are averaged lower than the overall average at 100 K. The **G2** residues are associated with a higher B-value. Hence, the inherent flexibility as indicated by the crystal structure correlates with the disappearance of the NMR signals.

In summary, resonances from amino acids not in β-sheets, with side chains near the solvent and in flexible portions of the protein are likely to pass through coalescence at higher temperatures. These resonances are also generally strongly inhomogeneously broadened. Therefore, the solvent and the structural conditions have a strong effect on the coalescence temperature and the intensity of NMR signals at cryogenic temperatures.

Conclusion

In this study, we show the effects of slow cooling on ^{13}C NMR signals of hydrated SH3 in the temperature range from 293 to 95 K. Individual carbon resonances begin to broaden at temperatures below 253 K, but this depends on the individual resonance. Many signals split into several distinct narrow peaks, with a linewidth similar to that observed at room temperature.

Identical chemical shifts and resolution are observed after re-heating the sample. The broad appearance of the peaks is not caused by inadequate heteronuclear dipolar decoupling, nor is it caused by a simple increase in single resonance linewidth. Rather, the ability to perform hole-burning spectroscopy and the multiple narrow signals at 95 K shows that the broadening is inhomogeneous. We have interpreted the inhomogeneous broadening to be a result of multiple conformers populated within the sample. Furthermore, in the case of side-chain signals we are able to show that a closer proximity of side-chain atoms to the solvent and a high flexibility increases the probability of high temperature coalescence. Even within an amino acid type there are different coalescence behaviors. If different conformers are the source of the multiple cryogenic NMR-signals it is likely that side chains mobile at room temperature and surrounded by solvent are adopting more conformations than side chains pointing into the core of the domain. However, much faster cooling rates than the ones used in this study (1°/min–10°/s) might mitigate the inhomogeneous broadening.

In conclusion, cryogenic ssNMR spectroscopy offers enhancements in signal-to-noise, especially when used with DNP. New insights into structures and dynamics of biological systems are possible thanks to the different interaction timescale as compared to X-ray crystallography. It is feasible, if difficult, to obtain information on different structural conformations on the atomic scale. Due to the large amount of spectral overlap, techniques to resolve the numerous signals will be needed to perform more detailed investigations of the underlying processes. However, the possibility of large signal enhancements through DNP, improved sample stability, and the rich structural information available with cryogenic ssNMR will motivate many more investigations and advancements in the future.

Acknowledgments The authors would like to thank Anne Diehl and Kristina Rehbein for preparation of the SH3 sample, and Dr. Rasmus Linser for access to his solvent accessibility calculations. This work was supported by the Deutsche Forschungsgemeinschaft (SFB449), Structural Biology of Membrane Proteins (Award #211800), The European Drug Initiave on Channels and Transports (Award #201924), and Bio-NMR (Award # 261863).

References

Agarwal V, Faelber K, Hologne M, Chevelkov V, Oschkinat H, Diehl A, Reif B (2007) Comparison of MAS solid-state NMR and X-ray crystallographic data in the analysis of protein dynamics in the solid state. To be Published

Akbey Ü, Oschkinat H, van Rossum B (2009) Double-nucleus enhanced recoupling for efficient 13C MAS NMR correlation spectroscopy of perdeuterated proteins. J Am Chem Soc 131:17054–17055

Akbey Ü, Lange S, Franks WT, Linser R, Rehbein K, Diehl A, van Rossum B, Reif B, Oschkinat H (2010a) Optimum levels of exchangeable protons in perdeuterated proteins for proton detection in MAS solid-state NMR spectroscopy. J Biomol NMR 46:67–73

Akbey Ü, Franks WT, Linden A, Lange S, Griffin RG, Rossum BV, Oschkinat H (2010b) Dynamic nuclear polarization of deuterated proteins. Angew Chem Int Ed 49:7803–7806

Bajaj VS, van der Wel PCA, Griffin RG (2009) Observation of a low-temperature, dynamically driven structural transition in a polypeptide by solid-state NMR spectroscopy. J Am Chem Soc 131:118–128

Barnes AB, Mak-Jurkauskas ML, Matsuki Y, Bajaj VS, van der Wel PCA, Derocher R, Bryant J, Sirigiri JR, Temkin RJ, Lugtenburg J, Herzfeld J, Griffin RG (2009) Cryogenic sample exchange NMR probe for magic angle spinning dynamic nuclear polarization. J Magn Reson 198:261–270

Bloembergen N (1949) On the interaction of nuclear spins in a crystalline lattice. Physica 15:386–426

Caliskan G, Briber RM, Thirumalai D, Garcia-Sakai V, Woodson SA, Sokolov AP (2006) Dynamic transition in tRNA is solvent induced. J Am Chem Soc 128:32–33

Castellani F, van Rossum B, Diehl A, Schubert M, Rehbein K, Oschkinat H (2002) Structure of a protein determined by solid-state magic-angle-spinning NMR spectroscopy. Nature 420: 98–102

Castellani F, van Rossum B, Diehl A, Rehbein K, Oschkinat H (2003) Determination of solid-state NMR structures of proteins by means of three-dimensional 15 N–13C-13C dipolar correlation spectroscopy and chemical shift analysis. Biochemistry 42: 11476–11483

Chevelkov V, Faelber K, Diehl A, Heinemann U, Oschkinat H, Reif B (2005) Detection of dynamic water molecules in a microcrystalline sample of the SH3 domain of alpha-spectrin by MAS solid-state NMR. J Biomol NMR 31:295–310

Debye P (1913) Interferenz von Röntgenstrahlen und Wärmebewegung. Ann Phys 348:49–92

Franks WT, Zhou DH, Wylie BJ, Money BG, Graesser DT, Frericks HL, Sahota G, Rienstra CM (2005) Magic-angle spinning solid-state NMR spectroscopy of the beta1 immunoglobulin binding domain of protein G (GB1): 15 N and 13C chemical shift assignments and conformational analysis. J Am Chem Soc 127:12291–12305

Franks WT, Wylie BJ, Schmidt HLF, Nieuwkoop AJ, Mayrhofer R, Shah GJ, Graesser DT, Rienstra CM (2008) Dipole tensor-based atomic-resolution structure determination of a nanocrystalline protein by solid-state NMR. Proc Nat Acad Sci USA 105:4621–4626

Gansmüller A, Concistrè M, McLean N, Johannessen OG, Marín-Montesinos I, Bovee-Geurts PHM, Verdegem P, Lugtenburg J, Brown RCD, Degrip WJ, Levitt MH (2009) Towards an interpretation of (13)C chemical shifts in bathorhodopsin, a functional intermediate of a G-protein coupled receptor. Biochim Biophys Acta 1788:1350–1357

Goddard TD, Kneller DG, University of California, San Francisco. SPARKY 3

Heise H, Hoyer W, Becker S, Andronesi OC, Riedel D, Baldus M (2005) Molecular-level secondary structure, polymorphism, and dynamics of full-length alpha-synuclein fibrils studied by solid-state NMR. Proc Nat Acad Sci USA 102:15871–15876

Hu K, Havlin RH, Yau W, Tycko R (2009) Quantitative determination of site-specific conformational distributions in an unfolded protein by solid-state nuclear magnetic resonance. J Mol Biol 392:1055–1073

Jehle S, van Rossum B, Stout JR, Noguchi SM, Falber K, Rehbein K, Oschkinat H, Klevit RE, Rajagopal P (2009) AlphaB-crystallin: a hybrid solid-state/solution-state NMR investigation reveals structural aspects of the heterogeneous oligomer. J Mol Biol 385:1481–1497

Jehle S, Rajagopal P, Bardiaux B, Markovic S, Kühne R, Stout JR, Higman VA, Klevit RE, van Rossum B, Oschkinat H (2010) Solid-state NMR and SAXS studies provide a structural basis for the activation of [alpha]B-crystallin oligomers. Nat Struct Mol Biol 17:1037

Kriminski S, Kazmierczak M, Thorne RE (2003) Heat transfer from protein crystals: implications for flash-cooling and X-ray beam heating. Acta Crystallogr Sect D 59:697–708

Lange A, Becker S, Seidel K, Giller K, Pongs O, Baldus M (2005) A concept for rapid protein-structure determination by solid-state NMR spectroscopy. Angew Chem Int Ed 44:2089–2092

Lesage A, Lelli M, Gajan D, Caporini MA, Vitzthum V, Miéville P, Alauzun J, Roussey A, Thieuleux C, Mehdi A, Bodenhausen G, Copéret C, Emsley L (2010) Surface enhanced NMR spectroscopy by dynamic nuclear polarization. J Am Chem Soc 132: 15459–15461

Linser R, Fink U, Reif B (2009) Probing surface accessibility of proteins using paramagnetic relaxation in solid-state NMR spectroscopy. J Am Chem Soc 131:13703–13708

Lipton AS, Heck RW, de Jong WA, Gao AR, Wu X, Roehrich A, Harbison GS, Ellis PD (2009) Low temperature 65Cu NMR spectroscopy of the Cu+ site in azurin. J Am Chem Soc 131:13992–13999

Loquet A, Bardiaux B, Gardiennet C, Blanchet C, Baldus M, Nilges M, Malliavin T, Böckmann A (2008) 3D structure determination of the Crh protein from highly ambiguous solid-state NMR restraints. J Am Chem Soc 130:3579–3589

Maricq M, Waugh J (1979) NMR in rotating solids. J Chem Phys 70:3300–3316

Mills J, Dean P (1996) Three-dimensional hydrogen-bond geometry and probability information from a crystal survey. J Comput Aided Mol Des 10:607–622

Morcombe CR, Zilm KW (2003) Chemical shift referencing in MAS solid state NMR. J Magn Reson 162:479–486

Ngai KL, Capaccioli S, Shinyashiki N (2008) The protein "glass" transition and the role of the solvent. J Phys Chem B 112: 3826–3832

Pauli J, Baldus M, van Rossum B, de Groot H, Oschkinat H (2001) Backbone and side-chain 13C and 15 N signal assignments of the alpha-spectrin SH3 domain by magic angle spinning solid-state NMR at 17.6 Tesla. ChemBioChem 2:272–281

Petkova AT, Ishii Y, Balbach JJ, Antzutkin ON, Leapman RD, Delaglio F, Tycko R (2002) A structural model for Alzheimer's beta -amyloid fibrils based on experimental constraints from solid state NMR. Proc Nat Acad Sci USA 99:16742–16747

Pettersen EF, Goddard TD, Huang CC, Couch GS, Greenblatt DM, Meng EC, Ferrin TE (2004) UCSF Chimera-a visualization system for exploratory research and analysis. J Comput Chem 25:1605–1612

Roh JH, Novikov VN, Gregory RB, Curtis JE, Chowdhuri Z, Sokolov AP (2005) Onsets of anharmonicity in protein dynamics. Phys Rev Lett 95:038101

Siemer AB, Huang K, McDermott AE (2010) Protein-ice interaction of an antifreeze protein observed with solid-state NMR. Proc Natl Acad Sci USA 107:17580–17585

Spiess H (1985) Deuteron NMR—a Nes tool for studying chain mobility and orientation in polymers. Adv Polym Sci 66:23–58

Szeverenyi N, Sullivan M, Maciel G (1982) Observationof spin exchange by two-dimensional fourier-transform C-13 cross polarisation-magic-angle-spinning. J Magn Reson 47:462–475

Thurber KR, Tycko R (2008) Biomolecular solid state NMR with magic-angle spinning at 25 K. J Magn Reson 195:179–186

Thurber KR, Tycko R (2009) Measurement of sample temperatures under magic-angle spinning from the chemical shift and spin-lattice relaxation rate of (79)Br in KBr powder. J Magn Reson 196:84–87

Vugmeyster L, Ostrovsky D, Ford JJ, Lipton AS (2010) Freezing of dynamics of a methyl group in a protein hydrophobic core at cryogenic temperatures by deuteron NMR spectroscopy. J Am Chem Soc 132:4038–4039

Waller I (1923) SpringerLink—Zeitschriftenbeitrag. Z Phys A At Nucl 17:398–408

Wasmer C, Lange A, Melckebeke HV, Siemer AB, Riek R, Meier BH (2008) Amyloid fibrils of the HET-s(218–289) prion form a beta solenoid with a triangular hydrophobic core. Science 319: 1523–1526

Zech SG, Wand AJ, McDermott AE (2005) Protein structure determination by high-resolution solid-state NMR spectroscopy: application to microcrystalline ubiquitin. J Am Chem Soc 127: 8618–8626

Zhou DH, Shah G, Cormos M, Mullen C, Sandoz D, Rienstra CM (2007) Proton-detected solid-state NMR spectroscopy of fully protonated proteins at 40 kHz magic-angle spinning. J Am Chem Soc 129:11791–11801